A New Low Switching Frequency Control of Regenerative CHB Drive With Low-Voltage Ride-Through Capability

Zhituo Ni, *Member, IEEE*, Ahmed H. Abuelnaga, *Member, IEEE*, Sarah Badawi, *Student Member, IEEE*, Shaoyi Yuan, Mehdi Narimani, *Senior Member, IEEE*, Ahmed Sayed-Ahmed, *Senior Member, IEEE*, Zhongyuan Cheng, *Senior Member, IEEE*, and Navid R. Zargari, *Fellow, IEEE*

***Abstract*—In conventional medium-voltage high-power cascaded H-bridge (CHB) drive, a three-phase rectifier is adopted in each power cell to provide isolated dc-bus voltage for the output H-bridge. This limits the application of the conventional CHB drive, where regeneration capability is desired. The regenerative CHB drive can be made possible by replacing the diode rectifier with a three-phase IGBT-based active-front-end (AFE) rectifier in each power cell. However, due to thermal constraints in the high-power medium-voltage drives, the first challenge of the regenerative CHB drive is to deal with the extra switching losses introduced by the IGBT devices. Another challenge of the grid-tied regenerative CHB drive is to handle the low-voltage sags in the power grid without triggering unnecessary downtime in transients. In this article, a novel low-switching frequency control strategy is proposed for the AFEs in the regenerative CHB drive with low-voltage ride-through (LVRT) capability. The main harmonic contents generated by the AFEs with the proposed control strategy can be eliminated by the existing phase-shifting transformer in the CHB drives. This allows meeting with IEEE STD 519-2014 requirement with a 60 Hz switching frequency to minimize the extra introduced switching losses in steady state. Moreover, LVRT capability is integrated into the proposed control scheme with reduced current sensor count. Accompanied with videos, the experiments on a seven-level regenerative CHB drive are implemented to validate the feasibility of the proposed control scheme, which can be extended to regenerative CHB drives with any voltage levels.**

***Index Terms*—Low grid voltage ride-through, low-frequency modulation strategy, multilevel regenerative drives.**

Manuscript received 11 May 2022; revised 24 August 2022; accepted 9 October 2022. Date of publication 20 October 2022; date of current version 18 November 2022. This work was supported by the Rockwell Automation Canada and Natural Sciences and Engineering Research Council of Canada (NSERC). Recommended for publication by Associate Editor M. Tavakoli Bina. *(Corresponding author: Zhituo Ni.)*

Zhituo Ni, Ahmed H. Abuelnaga, Zhongyuan Cheng, and Navid R. Zargari are with the Rockwell Automation Inc., Cambridge, ON N1R 5N9, Canada (e-mail: zhituoni@gmail.com; abuelnaa17@gmail.com; gcheng@ra.rockwell.com; nrzargari@ra.rockwell.com).

Sarah Badawi, Shaoyi Yuan, and Mehdi Narimani are with the Department of Electrical and Computer Engineering, McMaster University, Hamilton, ON L8S 4L8, Canada (e-mail: badaws1@mcmaster.ca; yuans20@mcmaster.ca; narimanm@mcmaster.ca).

Ahmed Sayed-Ahmed is with the Rockwell Automation Inc., Milwaukee, WI 53204 USA (e-mail: asahmed@ra.rockwell.com).

Color versions of one or more figures in this article are available at https://doi.org/10.1109/TPEL.2022.3216001.

Digital Object Identifier 10.1109/TPEL.2022.3216001

I. Introduction

ELECTRIC motor systems are by far the most important type of load in industry, using about 70% of the consumed electricity in the European Union [1], [2]. Medium-voltage (MV) high-power adjustable speed drives (ASD) have found widespread applications in various heavy industries, such as in the oil and gas sectors, production plants, and process industries [3], [4]. The conventional cascaded H-bridge (CHB) multilevel inverters prevailed in the MV industrial drive domain due to their modularity, scalability, and reliability [5], [6]. CHB inverter, shown in Fig. 1(a), is composed of a number of H-bridge power cells, which is cascaded on the motor side to achieve the full MV range with low harmonic distortion. In the conventional CHB drives, the isolated dc-bus voltages are obtained through a phase-shifting transformer and three-phase diode-front-end (DFE) rectifiers, which are shown in Fig. 1(b). The phase-shifting transformer can produce a set of three-phase secondary voltages shifted by a certain angle with respect to the primary voltages. The phase-shifting angles can eliminate low-order harmonics of the currents at the grid point of common coupling (PCC) with an improved harmonic profile [7].

However, conventional CHB drives rely on a brake resistor connected to the dc-bus to absorb the high power when negative torque is applied to the load motor. It is desirable to integrate the regenerative capability into the CHB drive that can reconvert the energy in the load motor back to the main power grid. This regeneration feature can bring a significant amount of energy saving in different industrial applications, such as conveyors, cranes, and other production lines, where frequent braking operation is required. According to the studies, with the adoption of the regenerative ASD system and efficient transmission in the lifts, the consumed energy can be reduced to 19% when compared to a conventional lift system using a pole changing drive [2]. Regeneration capability has become a standard technology for the new generation MV high-power CHB drive when constant braking is required.

One main challenge of designing an MV high-power regenerative CHB drive is to comply with the grid harmonic requirement code with a minimum switching loss in steady operations. On one hand, as the current harmonics generated by the regenerative CHB drive are directly fed back into the grid, it may disrupt other

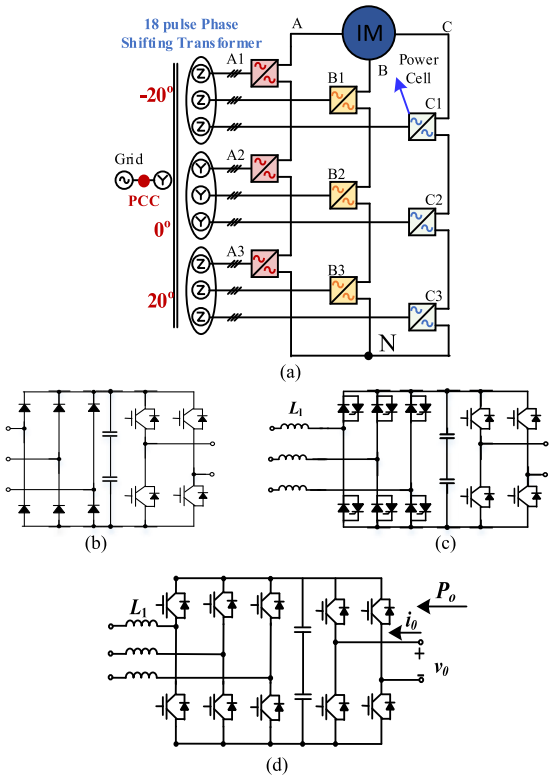

Fig. 1. Seven-level regenerative CHB drive. (a) CHB configuration. (b) DFE (non-Regen) power cell. (c) SCR Regen power cell. (d) IGBT-based AFE Regen power cell.

types of equipment if excess current harmonics are present. The current harmonics on the PCC shown in Fig. 1(a) are required to comply with recommended practice outlined by IEEE std 519–2014 [8], where a maximum total harmonic distortion (THD) of 5% is allowed. On the other hand, the thermal constraints of semiconductor devices and cooling system design impose limits on the introduced power losses for high-power converters [9]. In high-power applications, the IGBT device switching frequency $f_{\rm sw}$ is normally limited up to 500–600 Hz [10].

Different versions of MV regenerative CHB drive had been proposed so far targeting a good harmonic profile with the minimum switching loss. One promising solution [11], [12] is to introduce a six-pulse thyristor phase-controlled SCR inverter in each power cell to an existing DFE CHB power cell, which is illustrated in Fig. 1(c). The main benefit of the SCR inverter solution is that almost all the low-frequency harmonics generated by the SCR inverter during regeneration, such as 5th, 7th, 11th, and 13th harmonic components, can be eliminated by the existing phase-shifting transformer in the motoring and regeneration. However, SCR being a semi-controlled device, once the anode current is above the holding current, the gate loses control. It cannot be turned OFF until the occurrence of the next zero crossing of the anode current. The safe commutation of the SCR cannot be guaranteed during the grid voltage sag [13].The upper leg SCR may be triggered before closing the bottom leg SCR (pending on the zero current crossings) and thus results in dc-bus short circuit. Another popular solution [14], [15] is to adopt the IGBT active front end (AFE) instead of the DFE rectifier in each CHB power cell, as is shown in Fig. 1(d). During the motoring operation, the back-diodes of the IGBT are operated similar to the DFE rectifiers to provide the isolated dc voltages for the power cells with no additional switching loss. The IGBTs only start to switch and deliver the suitable energy from the motor side to the grid in regeneration intervals [16]. The conventional *dq* frame control schemes of the AFE based on SPWM and SVM are widely used in [17] and [18]. To eliminate the switching sideband harmonics generated by the SPWM, an asymmetric carrier-shifting SPWM method is proposed for the regenerative CHB drive in [19] satisfying the demand of the IEEE std 519-2014 with a 900 Hz switching frequency. But the limitation of the SPWM method lies in that it can lead to unacceptably low-order harmonics when operating at a very low device switching frequency $f_{\rm sw}$ [9], [20], which is not desirable for the high-power regenerative CHB drives where a low switching frequency is demanded.

Other existing low switching frequency control strategies, such as selective harmonic mitigation PWM [21], synchronous optimal PWM strategy [22], and the model predictive pulse pattern control [23] had been proposed for the multilevel neutral-point clamped (NPC) drives to remove the low-order harmonics. However, unlike the NPC drive, all these methods are not suitable for the regenerative CHB drives because the existing phase-shifting transformer in the regenerative CHB drive can naturally eliminate low-order harmonics. There is a need for a harmonic-friendly low-switching frequency control strategy optimized for the regenerative CHB drive where the phase-shifting transformer is presented.

Another critical challenge of the regenerative CHB drive is to handle momentary voltage disturbances in the power grid without triggering unnecessary downtime [2]. More than 62% of the disturbances recorded in the grid disturbances were voltage sags with a duration of less than 0.5 s according to the studies in [24]. A momentary voltage sag can trigger an immediate overcurrent tripped out in the AFEs and cause a significant loss in revenue and costly downtime. Industries have reported losses ranging from $10 000 to $1 000 000 per disrupting event [25]. These losses can be significantly reduced for critical production processes by integrating ride-through capabilities in the new regenerative CHB drive according to IEEE std 1566-2015 [26]. As is described in IEEE std 1566-2015, the drive system shall ride through and maintain control of the motor during an input power voltage sag down to 65% of nominal for a duration of 500 ms. Although some work [25], [27] has been done on the low-voltage ride through in the ASDs, no work has been found on the MV regenerative CHB drive which usually operates with a very low switching frequency.

To tackle the previous illustrated two challenges, this article proposed an advanced controller for the IGBT-based regenerative CHB drive, shown in Fig. 1(d), that can comply with the IEEE std 519-2014 harmonic requirement with fundamental switching frequency (FSF) in steady operation state and meanwhile have the extended low-voltage ride-through (LVRT) capability for momentary transient operations.

The contributions of the proposed control strategy can be substantialized as follows:

1) In steady-state operation, a good harmonic profile that complies with IEEE std 519-2014 is achieved with a low switching frequency $f_{\rm sw}$ at 60 Hz, which cannot be done with existing SPWM control strategies under the same switching frequency.
2) Unlike the SCR-frond-end solutions, the transient LVRT capability can be obtained by integrating the current hysteresis controller with the proposed switching frequency method. The hysteresis switching is only activated during momentary operation providing high control bandwidth during voltage sags.
3) Moreover, to further reduce the system cost, a dc-bus current estimator is proposed based on the IGBT gratings and phase currents to reduce one current sensor in each power cell of the regenerative CHB drives.

Section II introduces the proposed FSF control strategy. Section III demonstrates the proposed FSF control with the extension of the LVRT capability. The proposed control strategy is verified on a seven-level CHB drive experiment setup in Section IV. Finally, conclusions are drawn in Section V.

II. Proposed FSF Controller and Limitation

Unlike the other IGBT-based AFE control strategies based on *dq* rotating frame, in this article, the AFE IGBTs work in a manner similar to the "thyristors" in the phase-controlled SCR inverter shown in Fig. 1(c). Without introducing extra switching sideband harmonics, the main advantage of the proposed FSF control strategy is that the harmonic contents generated by the AFE are at a low-order harmonics range, such as 5th, 7th, 11th, and 13th harmonic frequencies, which can be further eliminated by the existing phase-shifting transformer. This superb merit allows satisfying the harmonic requirement IEEE std 519-2014 with the FSF, which is desirable for the MV high-power regenerative CHB drives. In this section, the harmonic cancellation mechanism of the phase-shifting transformer is first analyzed. Then the FSF control strategy ($f_{\rm sw} = 60$ Hz) is introduced for the regenerative power cell. Without losing the generality, the proposed control scheme is studied based on a seven-level regenerative CHB drive. It can be further extended to other regenerative CHB drives due to the modular power cell structure.

A. Harmonic Cancellation of Phase-Shifting Transformer

Special attention had to be paid to the fact that a number of regenerative power cells are parallel connected to the grid via a phase-shifting transformer. A number of low-order harmonics generated by the AFEs can be naturally removed by the existing phase-shifting transformer. In a conventional MV CHB drive, the phase-shift among the secondary windings of a typical phase-shifting transformer can be formulated as $60°/N_s$, where $N_{\rm s}$ is the number of the cascaded power cell in each phase of the CHB drive. For example, as is shown in Fig. 1(a), three power cells are cascaded in each phase ($N_s = 3$) for a seven-level CHB drive with an 18-pulse phase-shifting transformer. In the 18-pulse phase-shifting transformer, a 20° (60°/3) phase angle displacement is between any two adjacent secondary windings in each phase. Four dominant harmonics (the 5th, 7th, 11th, and 13th) can be naturally eliminated by the 18-pulse phase-shifting transformer in the seven-level CHB drive [3]. Recently, a new 54-pulse phase-shifting transformer is obtaining more and more attention for seven-level CHB drives by introducing an extra 6.7° phase-shift among the power cells in different phases [28]. All harmonics below 50th can be eliminated by the 54-pulse phase-shifting.

B. Proposed FSF Control Diagram for AFE

As the IGBTs in the AFE work in a similar manner to the "thyristors" in the SCR inverter, as is shown in Fig. 2(a), the FSF control strategy for the AFE is developed from the SCR inverter control scheme. Specifically, in regeneration operation, the regeneration power comes from the motor and flows into the dc bus through the H-bridge in each power cell. The firing angle and conduction angle of each IGBT in AFE are controlled and regulated in a pattern to deliver a suitable amount of power into the grid to prevent hitting the dc-bus overvoltage limit.

As is shown in Fig. 2(a), when the power flow back from the load raises up the dc-bus voltage $u_{\rm dc}$, the dc voltage PI regulator will increase the average dc-bus current $I_{\rm dc0\cdot ref}$ reference flowing from the dc bus into the AFE inverter. The dc-bus current PI regulator will respond to this reference change and increase the average dc-bus current $I_{\rm dc0}$ by adjusting the IGBTs firing angle α in the switching pattern in the AFEs, delivering more power from the dc bus to the grid and stabilizing the dc-bus average voltage at its defined reference $u_{\rm dc0\cdot ref}$.

The proposed switching pattern modulator is shown in Fig. 2(b), where the IGBTs in the AFE are labeled as *S*1 to *S*6. The opening of the upper leg A-phase IGBT *S*1 is delayed by the firing angle α degree from the zero-crossing point of the A-phase voltage. The conduction angle ϕ of each AFE IGBT is 120^0. The same rule applies to the upper leg IGBT *S*3 and *S*5 in the B-phase and C-phase. The bottom leg IGBTs *S*4, *S*6, and *S*2 gating signals are 180° delayed from their counterpart upper leg IGBTs *S*1, *S*3, and *S*5, respectively. Therefore, there are six switching states where two out of six IGBT switches are ON states: 61, 12, 23, 34, 45, and 56. With this switching pattern, by adjusting the firing angle α, different average dc-bus current $I_{\rm dc0}$ can be injected into the grid through the AFE. In the steady state, the average power delivered to the grid by the AFE equals the average power coming from the H-bridge. The desired average dc-bus output current to the AFE is

$$I_{\rm dc0} = \frac{\mathrm{Re}\left(\mathbf{v_o}\mathbf{i_o^*}\right)}{u_{\rm dc0}} \tag{1}$$

where $\mathbf{v_o}$ is the H-bridge output voltage phasor and $\mathbf{i_o^*}$is the conjugate of the H-bridge output current phase vector. $u_{\rm dc0}$ is the average dc-bus voltage of the AFE.

Instead of controlling the 60 Hz ac current injected into the grid by each AFE based on *dq* rotating frames, the proposed FSF method controls the average dc-bus current $I_{\rm dc0}$ through the AFE to stabilize the dc-bus voltage during regeneration with a FSF.

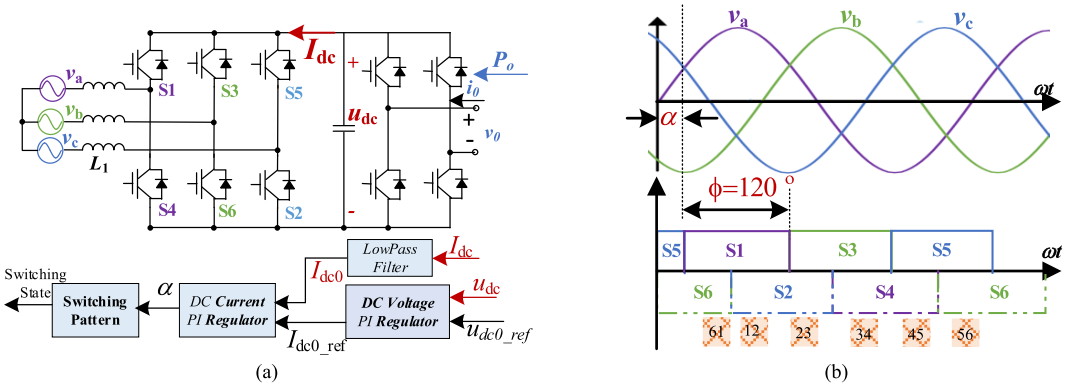

Fig. 2. Fundamental switching frequency control for AFE. (a) Control scheme. (b) Switching pattern.

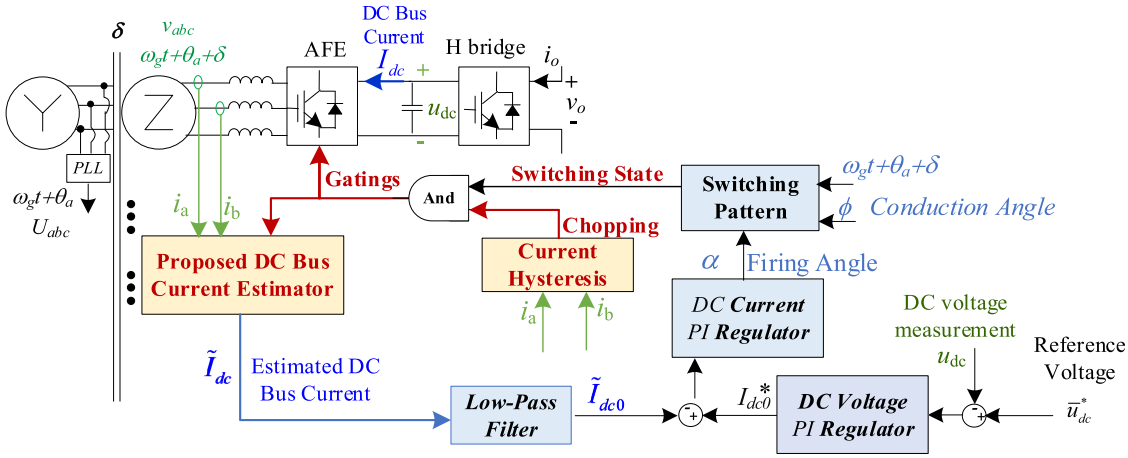

Fig. 3. Proposed FSF control for regenerative CHB drive with low-voltage ridge-through capability enhancement.

III. Proposed FSF Control With Low-Voltage Ride-Through Capability Enhancement

As is shown in Fig. 2, low-pass filter and PI regulators are adopted in the FSF controller offering the particular benefit of controlling a constant dc-bus voltage by adjusting the firing angle. However, this controller has a limited control bandwidth for dynamic performance. When the grid voltage sag happens, the controller shown in Fig. 2 cannot respond in time to suppress the peak current of the phase currents at the input of the regenerative power cell and thus triggering an immediately overcurrent downtime. This is not desirable and must be considered in industry applications. In this section, LVRT capability is extended into the proposed FSF control scheme during the grid voltage sags.

A. Proposed Control Scheme

The proposed FSF controller with LVRT enhancement is shown in Fig. 3. In order to get a quick response under grid voltage sags transient, a hysteresis band current controller is introduced with the input phase currents to generate the chopping signals. The IGBT gatings are created by AND operation between the switching state determined by the FSF controller and the chopping signal from the current hysteresis controller.

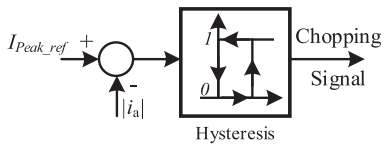

Fig. 4. Hysteresis band current controller.

The implementation of the hysteresis controller on A-phase current is shown in Fig. 4 [29]. When A-phase current i_a amplitude reaches the allowable peak current $I_{\text{peak'ref}}$, the chopping signals for IGBT S_1 and S_4 are zero. With S_1 and S_4 gating closed, A-phase current will decrease until triggering the hysteresis band. This hysteresis band current control can provide the AFE with an extremely high control bandwidth during the grid voltage sag intervals. Although the hysteresis chopping signal may introduce a high switching loss. However, this is not a problem as most grid voltage sag will only last for a few cycles such as duration of 500 ms stipulated in the IEEE std 1566-2015.

B. Proposed DC-Bus Current Estimator

As previously discussed, to obtain the LVRT capability, extra two current sensors are required to be added in each power cell

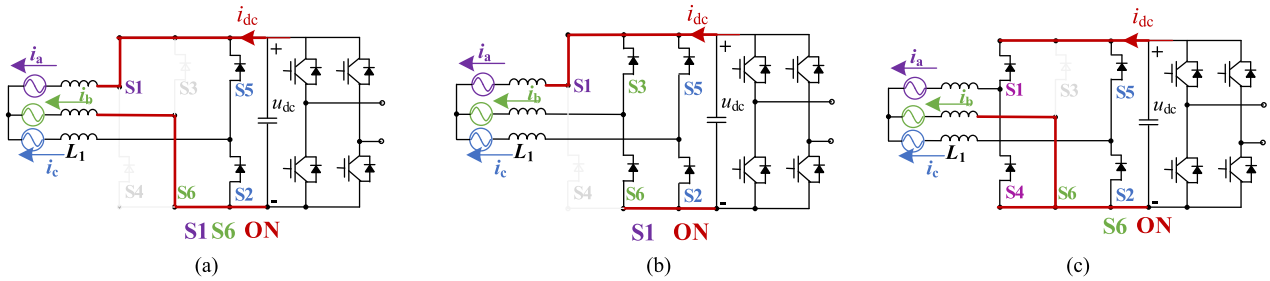

Fig. 5. S_1, S_6 switching state for DC-bus current estimation. (a) S_1S_6 ON. (b) Only S_1 ON. (c) S_6 ON.

for implementing the current hysteresis band controller. Meanwhile, as is shown in Fig. 2, the dc-bus current is also required to be measured for the FSF controller. To reduce the number of the total current sensors, as is shown in Fig. 3, instead of adding an extra dc-bus current sensor, the dc-bus current is real-time estimated through the proposed dc-bus current estimator based on the AFE IGBT gatings and input phase currents.

There are six switching states in the switching pattern from the proposed FSF controller shown in Fig. 2. When S_1, S_6 switches are ON state, as is shown in Fig. 5(a). If the C-phase current i_c is positive flowing through the back-diode of IGBT S_2, then the dc-bus current $\tilde{i}_{dc}$equals the A-phase current i_a due to Kirchhoff's current law (KCL). On the other hand, if C-phase current i_c is reversed, the diode in S_5 IGBT is conducted. The dc-bus current $\tilde{i}_{dc}$equals the B-phase current $-i_b$ based on KCL. As a result, when S_1, S_6 switches are ON, the estimated dc-bus current $\tilde{i}_{dc}$can be calculated depending on the C-phase current i_c direction

$$\tilde{i}_{dc} = \begin{cases} i_a & \text{if} i_c > 0 \\ -i_b & \text{if} i_c \le 0. \end{cases} \tag{2}$$

During the grid voltage sag interval, S_1 or S_6 may be closed by the introduced hysteresis band current controller when A-phase or B-phase current reaches the allowable maximum current. When S_6 is turned OFF by the B-phase hysteresis current controller during the grid voltage sag interval, as is shown in Fig. 5(b) with only S_1 ON, the dc-bus current in this situation can be estimated based on the B- and C-phase current direction

$$\tilde{i}_{dc} = \begin{cases} i_a & \text{if } i_b > 0 \text{ and } i_c > 0 \\ 0 & \text{if } i_b < 0 \text{ and } i_c < 0 \\ -i_b & \text{if } i_b \ge 0 \text{ and } i_c < 0 \\ -i_c & \text{if } i_b < 0 \text{ and } i_c \ge 0. \end{cases} \tag{3}$$

As is indicated in (3), based on the current directions in the B- and C-phase, the conduction of the back-diodes in the B- and C-phase IGBTs can be determined. After determining the back-diodes conduction conditions, the dc-bus current can be calculated through the KCL.

Similarly, when S_1 is turned OFF by the A-phase hysteresis current controller during the grid voltage sag interval, as is shown in Fig. 5(c) with only S_6 ON, the estimated dc-bus current $\tilde{i}_{dc}$can be calculated depending on the A- and C-phase currents directions

$$\tilde{i}_{dc} = \begin{cases} 0 & \text{if } i_a > 0 \text{ and } i_c > 0 \\ -i_b & \text{if } i_a < 0 \text{ and } i_c < 0 \\ i_c & \text{if } i_a \ge 0 \text{ and } i_c < 0 \\ i_a & \text{if } i_a < 0 \text{ and } i_c \ge 0. \end{cases} \tag{4}$$

TABLE I
SEVEN-LEVEL REGENERATIVE CHB DRIVE EXPERIMENT

Converter parameter	Value
Cell average dc-link voltage	110 V
Transformer primary side voltage (grid)	240 V
Transformer primary side voltage	80V
Grid-tied inductance	4 mH
Current sampling time	10 kHz
Current hysteresis band	[9 A, 14 A]
DC-link capacitance	4700 μF

The dc-bus current is now estimated during the S_1, S_6 switching ON state through (2)–(4). A similar analysis can be applied to the other five switching states12, 23, 34, 45, and 56. The dc-bus current can be reliably estimated through the proposed current estimator reducing the number of the required current sensors in the system.

IV. VALIDATION AND DISCUSSION

To validate the feasibility of the proposed FSF control scheme with LVRT capability, an experimental prototype is built based on a seven-level regenerative CHB drive. As shown in Fig. 6, an ABB ACS800 regenerative drive is operated in the torque mode to provide negative load torque to one of the back-to-back induction machines. A seven-level regenerative CHB drive with an 18-pulse phase-shifting transformer is to control the other induction machine. The regenerative power will flow from the load machine to the NHR 9340 grid simulator through the regenerative CHB drive. An induction motor control algorithm is implemented in the dSpace controller. A TI DSP28379d is adopted for each regenerative power cell implementing the proposed FSF control algorithm. Fluke 438 power quality analyzer is used to provide accurate harmonics and THD measurement. System parameters are shown in Table I.

A. Steady-State Performance

The proposed FSF control strategy ($f_{sw} = 60$ Hz) with LVRT capability is implemented on the illustrated seven-level regenerative CHB drive experimental platform. To reduce the sensor number, the dc-bus current i_{dc} is estimated with the proposed current estimator based on the IGBT switching gating and measured phase currents. As is shown in Fig. 7, in a steady state, the estimated dc-bus current $\tilde{i}_{dc}$matches the measured dc-bus current i_{dc}. Compared with the measured dc-bus current

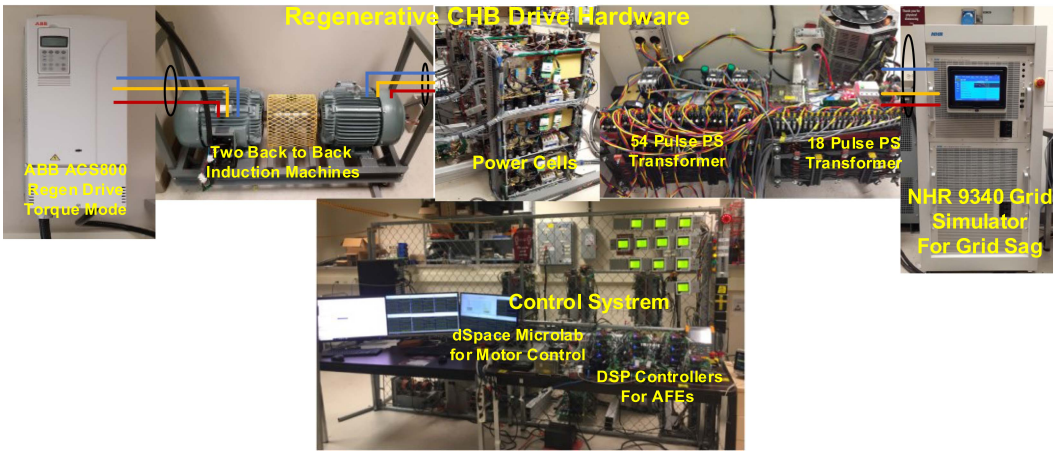

Fig. 6. Prototype of the seven-level CHB drive system.

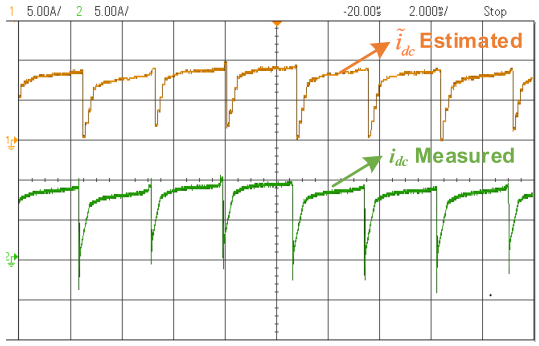

Fig. 7. DC bus current estimation and measurement.

i_{dc}, some small estimation error exists during IGBT switching transient due to the diode recovery effect and time-step limitation of the estimator implementation. However, as is shown in Fig. 3, it is not an issue since only the average dc-bus current $\tilde{I}_{\mathrm{dc0}}$is required to be used for the proposed FSF control. To obtain the dc component on the dc-bus current $\tilde{I}_{\mathrm{dc0}}$, a second-order 20 Hz bandwidth low-pass filter is adopted for the estimated dc-bus current $\tilde{i}_{\mathrm{dc}}$in the experiment.

With the proposed FSF control strategy, the phase currents I_a, I_b, and I_c generated by the AFE on the secondary side of the transformer are shown in Fig. 8(a) during the regeneration interval. The main harmonic contents generated by the AFE are mainly distributed at 5th, 7th, 11th, 13th, 17th, and 19$^{\mathrm{th}}$-order frequencies. This can be seen from the harmonic profile obtained from Fluke 438 shown in Fig. 8(b). A 10 V 120 Hz dc-bus voltage ripple is present in each regenerative power cell when the H-bridge outputs 60 Hz voltage to the load induction machine. With the proposed switching pattern at a 60 Hz switching frequency, the current THD generated by the AFE in each power cell reaches as high as 30%. However, this is not an issue since the main current harmonic contents generated by the AFE are positioned below 17th-order frequency which can be eliminated by the existing 18-pulse phase-shifting transformer among different power cells. As is shown in Fig. 8(c) and 8(d), with the main current harmonics eliminated by the transformer, the remaining harmonics components reflected to the primary side of the 18-pulse phase-shifting transformer are mainly 17th and 19th order. The THD at the PCC of the regenerative CHB drive is dramatically reduced to 4.7% with the switching frequency as low as 60 Hz. It is noted that, as shown in Fig. 8(d), there is an emerging third-order current harmonic only at the transformer's primary side due to the magnetizing current in the phase-shifting transformer.

TABLE II
54 PULSE PHASE-SHIFTING TRANSFORMER ILLUSTRATION

Transformer	A_1	A_1	A_1	B_1	B_2	B_3	C_1	C_2	C_3
18 Pulse (^{0})	−20	0	20	−20	0	20	−20	0	20
54 Pulse (^{0})	**−26.7**	**−6.7**	**13.3**	−20	0	20	**−13.3**	**6.7**	**26.7**

To further remove the 17th-order and 19th-order harmonics at the PCC, a 54 pulse-shifting transformer is further studied for the seven-level regenerative CHB drive in the experiment. As is shown in Fig. 1(a), the regenerative power cells in the CHB drives are labeled as Px, where P denotes A, B, and C phases and x denotes the cell number and can be 1,2,3, …,N. For example, A_1 denotes the first regenerative power cell in the A-phase. The secondary windings' phase-shifting angles of a 54-pulse transformer are shown in Table II. Compared with the conventional 18-pulse phase-shifting transformer, an extra 6.7° is introduced among the secondary windings in different phases [28].With the 54-pulse phase-shifting transformer, as is shown in Fig. 9, the THD at the PCC of the regenerative CHB drive is further reduced to 2.1%. Moreover, with the both 17th- and 19th-order harmonic removed, IEEE std 519-2014 can be fulfilled with an FSF (60 Hz), which is impossible with the existing SPWM control strategies.

B. Transition From Motoring to Regeneration

Unlike the conventional AFE controller based on *dq* rotating frame PWM methods, the proposed method keeps the AFE IGBTs OFF state during the whole motoring operation. The back-diodes of the AFE IGBTs are operated as three-phase diode rectifiers to provide the isolated dc-bus voltages for the power cells during motoring. It is equivalent to the conventional DFE

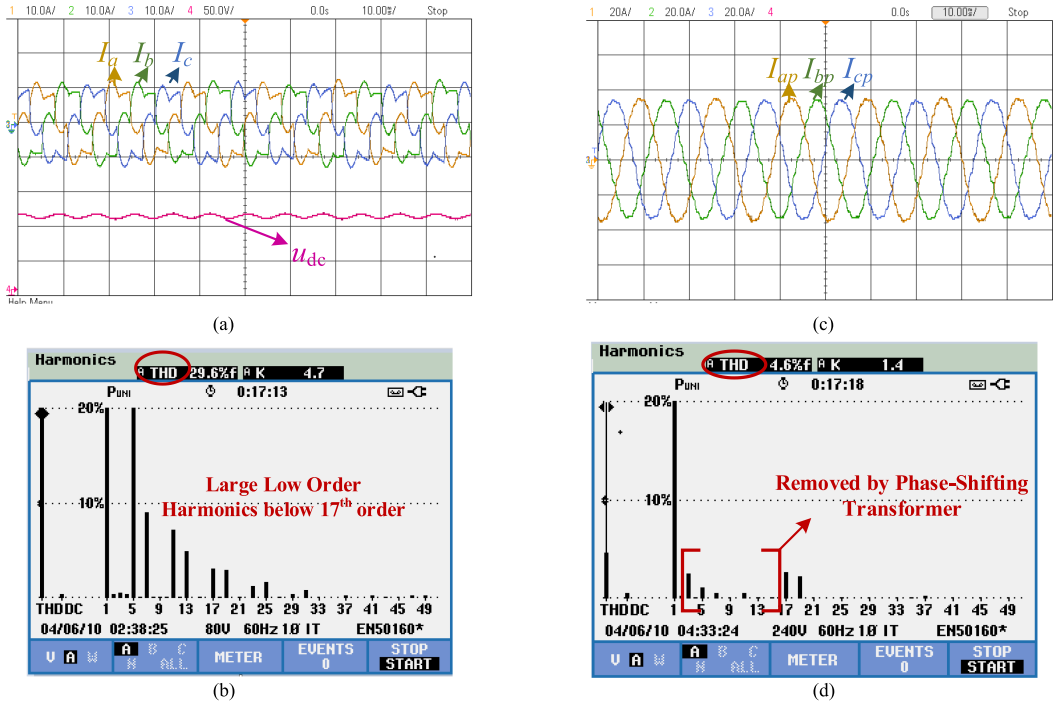

Fig. 8. Steady-state performance with 18 pulse phase-shifting transformer. (a) Transformer secondary side current. (b) Harmonics in secondary side current. (c) Transformer primary side current. (d) Harmonics in primary side current.

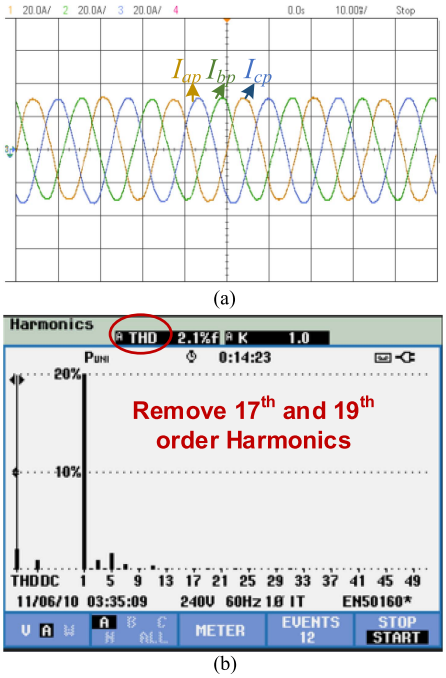

Fig. 9. Steady-state performance with 54 pulse phase-shifting transformer. (a) Transformer primary side current. (b) Harmonics in primary side current.

CHB drives. Only in regeneration operations, do the AFE IGBTs start to switch and deliver the suitable energy from the motor side to the grid to maintain a constant dc-bus voltage. In this way, the proposed method provides a better way of using the existing phase-shifting transformer in both motoring and regeneration operations with minimum loss.

The AFE output currents I_a, I_b, and I_c, and dc-bus voltage $u_{\rm dc}$ are shown in Fig. 10(a) during the transition from motoring to regeneration. As is shown in Fig. 10(a), during the motoring operation before t_1, the regenerative CHB drive is operated in a way similar to the conventional DFE CHB drive as the AFE IGBTs are at OFF state. The grid current I_{ap}, I_{bp}, I_{cp}, and line voltage $V_{\rm BC}$ are shown in Fig. 10(b), the transformer's primary side current is mainly the transformer magnetizing current since there is no torque load in motoring. After injecting the negative torque into the induction machine, energy flows back from the load machine to the regenerative power cells, and the dc-bus voltage in the power cell tends to increase. Once the dc-bus voltage hits the preset protection value at 130 V at t_1, the proposed FSF controller is then triggered, AFE IGBTs will then start to switch and deliver the energy from the machine side to the grid during regeneration at 60 Hz switching frequency. The proposed controller will bring back the dc-bus voltage to the reference value at 110 V, thus achieving a regeneration steady state. Harmonics of the grid currents are eliminated with the proposed FSF method in the steady state.

C. Dynamic Performance Under Grid Voltage Sag

As is previously illustrated, in the proposed FSF control scheme, extremely high control bandwidth is obtained by integrating the hysteresis band current controller to avoid unnecessary overcurrent downtime during the grid low-voltage sags. The AFE output currents $I_{\rm a}$, $I_{\rm b}$, and $I_{\rm c}$, and dc-bus voltage $u_{\rm dc}$ are shown in Fig. 11(a). The grid current I_{ap}, I_{bp}, I_{cp}, and line voltage $V_{\rm BC}$ are shown in Fig. 11(b). During the regeneration operation, the grid three-phase voltages at the primary side of

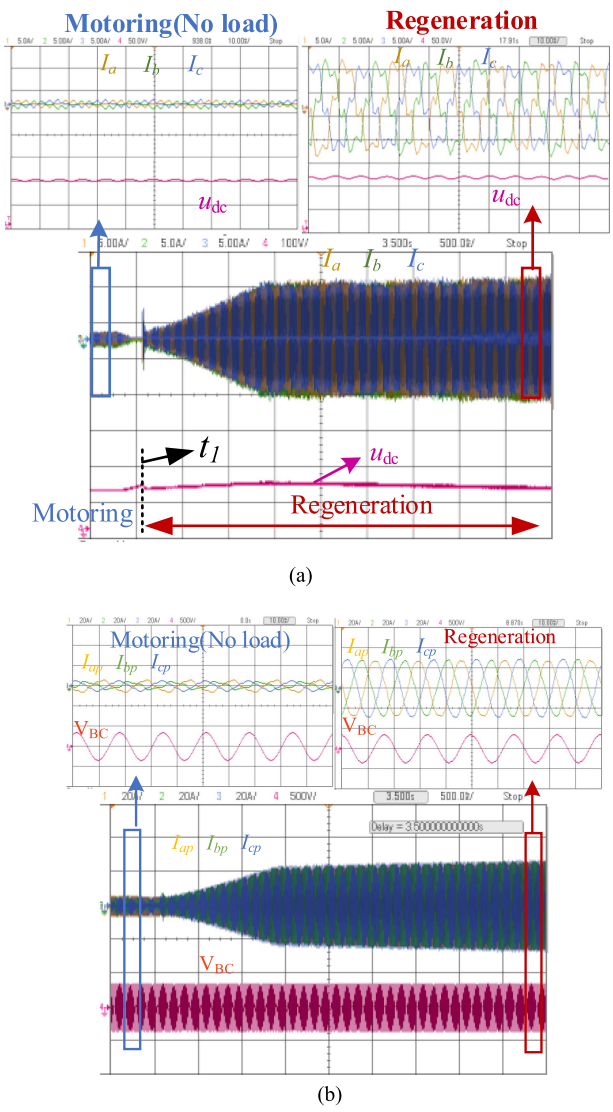

Fig. 10. Motoring to regeneration transition with the 54 pulse phase-shifting transformer. (a) Cell current and dc bus Voltage. (b) Transformer primary side current and line voltage.

the phase-shifting transformer are stepped down from 240 to 156 V by the grid simulator NHR 9340 at t_1, which is outlined by the IEEE std 1566-2015 [26]. The LVRT capability is studied with the proposed FSF control scheme. As is shown in Fig. 2, the inductors between the AFE and the transformer secondary winding suffer the voltage difference between the grid voltage and AFE output voltages. As the grid voltage drops immediately while the AFE output voltage remains the same at t_1 time step, it will lead to a high rush current on the inductor delivering increased power from the AFE to the grid, which is shown in Fig. 11(a). As the regeneration power coming from the load remains the same, the dc-bus voltage drops responding to the grid voltage sag. During the t_1 and t_2 grid voltage sag interval, as is shown in Fig. 11(c), the proposed dc voltage controller will try to stabilize the dc voltage around its given reference at 110 V by adjusting the reference current I^*_{dc0}through the dc voltage regulator. The firing angle α of IGBT S_1 in AFE is saturated to the limit at 60°. It is noted that the implementation of the dc-bus current PI controller is in the convention of the current-controlled SCR [30], where the firing angle increases when the dc-bus reference current is less than the measured dc-bus current. The simulation of the conventional dc-bus current control scheme can be achieved from [30].

As is shown in Fig. 11(a), the phase currents of the AFEs are required to be increased to deliver the same amount of regeneration power from the load to the grid during the voltage sag. The AFE phase currents may hit the maximum allowable peak current limit. The hysteresis current controller can provide a fast response to keep the maximum phase currents of the AFE below the allowable protection value by introducing extra chopping during the voltage sag interval. As is shown in Fig. 11(a), the hysteresis band is between [9 A, 14 A] and the switching frequency is around 240 Hz during the voltage sag intervals. Different hysteresis bands can be adopted based on the switching frequency limitation during the voltage sag transient. At t_2 time step in Fig. 11(b), the three-phase grid voltage at the primary side of the transformer is stepped back to normal at 240 V. The dc-bus voltage in the power cell increases immediately as less power is converted from the AFE to the grid during this transient. After that, the dc-bus voltage and three-phase current finally come back to a steady state. During the grid voltage sag intervals, the proposed controller responds in time to suppress the peak current of AFE below the protection limit at the input of each regenerative power cell avoiding triggering an immediate overcurrent downtime. It is noted that the hysteresis switching is only activated during the grid voltage sag transients, such as 500 ms outlined by the IEEE std 1566-2015. The system is forced to shut down due to grid fault if grid voltage sag persists.

D. Loss Comparison With Existing Control Strategies

The losses comparative study between the proposed strategy and existing SPWM control strategies has been conducted under the same requirement that IEEE std 519-2014 is met at the grid side of the regenerative CHB drives. A 1 MW, 3 kV, and seven-level regenerative CHB drive is designed for comparison. The dc-bus's total capacitance is 4700 μF (assume the total ESR is 10 mΩ). The FF200R17KE4 has been adopted for the AFE IGBTs. Infineon IPOSIM software was used to calculate devices' power losses and IGBT junction temperatures under different PWM strategies.

As is shown in Table III, the existing PWM control strategies [19], [31] require a minimum of 900 and 1980 Hz, respectively, to meet the IEEE std 519-2014 for a seven-level CHB drive. However, the proposed method dramatically brings the required switching frequency to 60 Hz meanwhile satisfying IEEE std 519-2014. This can result in a significant reduction in power losses and junction temperature in each power cell. This switching loss minimization in the proposed control strategy can lead to a reduction in the manufacturing cost of the regenerative CHB drives due to the reduced cooling requirement. Moreover, the proposed fundamental switching method will not sacrifice the dc voltage ripple compared with the conventional SPWM

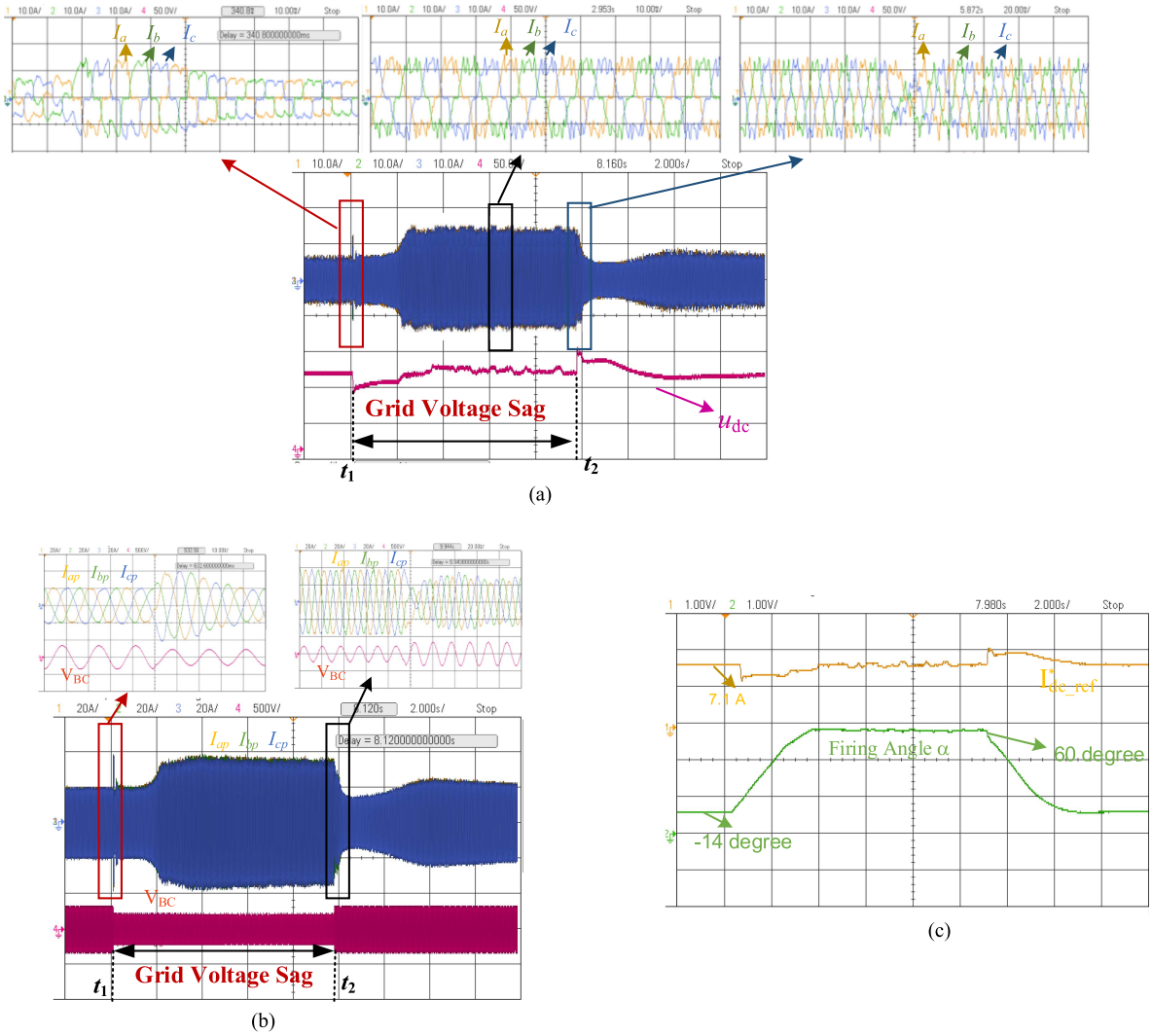

Fig. 11. Low voltage ride through performance. (a) Cell currents and dc bus voltage. (b) Grid current and voltage. (c) S_1 IGBT firing angle and DC current reference control signal.

TABLE III
AFE IGBT LOSS COMPARISON IN ONE POWER CELL MEETING IEEE STD 519-2014

Existing control strategy	Conventional SPWM method [31]	Asymmetrical carrier-shifted SPWM method [19]	Proposed method
Switching frequency (Hz)	1980	900	**60**
AFE IGBT losses in one power cell (W)	568.8	375.9	**257.7**
DC capacitor loss (W)	79.5	79.5	**80.6**
Max junction temperature (°C)	118	108	**101**

method [19], [31]. This is because the main component of the dc-bus voltage ripple is still twice the output frequency due to the structure of the CHB power cell [32]. The dc ripple caused by the control strategy is thus limited.

Compared with the conventional SCR-front-end solution [12], [33], with a similar dc-bus current control scheme [30], the proposed fundamental frequency control strategy can achieve a similar harmonic performance satisfying IEEE std 519-2014 at the grid PCC in steady state. More important is the fact that there is no potential commutation failure issue for the IGBT devices during the voltage sags. LVRT capability can be obtained with the proposed solution without adding additional power devices into the power cells [13], which is impossible with conventional SCR-front-end solutions [12], [33]. Beyond that, the dc-bus current is estimated with the proposed algorithm to further reduce the sensor count and system cost.

V. Conclusion

In this article, a new low switching frequency control strategy with extended LVRT capability is proposed for the high-power MV regenerative CHB drive. It allows operating the regenerative CHB drive at the 60 Hz switching frequency and meanwhile meeting the harmonic profile requirement IEEE std 519-2014 in steady-state operation. Moreover, the LVRT capability is integrated into the proposed controller by introducing hysteresis switching only in momentary operation. Beyond that, a dc-bus current estimator is proposed to further reduce the required current sensor count and cost.

To fully take advantage of the phase-shifting transformer, instead of controlling the injected ac current components based on the dq or $\alpha\beta$ frames in conventional grid connection strategies [19], [31], the proposed FSF method controls the average dc-bus current through the AFE to stabilize the dc-bus voltage during regeneration with a low switching frequency. With the proposed switching pattern, the main harmonics generated by the AFEs can be removed by the existing phase-shifting transformer in the regenerative CHB drive thus complying with the IEEE std 519-2014 at the PCC in steady operation. What is more, to avoid overcurrent downtime during the grid voltage sag, current hysteresis switching is integrated with the FSF control scheme. An extremely high control bandwidth is obtained to suppress the phase current during the momentary grid voltage sag. Beyond that, a dc-bus current estimator is proposed based on the IGBT gatings and phase currents to further reduce the number of the current sensors and thus reduce the system cost.

References

[1] "Actions to promote energy-efficient electric motors," in *SAVE Programme*, Motor Study Group. Brussels, Belgium: European DG, 1996.

[2] A. T. de Almeida, F. J. T. E. Ferreira, and D. Both, "Technical and economical considerations in the application of variable-speed drives with electric motor systems," *IEEE Trans. Ind. Appl.*, vol. 41, no. 1, pp. 188–199, Jan./Feb. 2005, doi: 10.1109/TIA.2004.841022.

[3] B. Wu and M. Narimani, *High-Power Converters and AC Drives*. Hoboken, NJ, USA: Wiley, 2017.

[4] J. Rodriguez, P. W. Hammond, J. Pontt, R. Musalem, P. Lezana, and M. J. Escobar, "Operation of a medium-voltage drive under faulty conditions," *IEEE Trans. Ind. Electron.*, vol. 52, no. 4, pp. 1080–1085, Aug. 2005.

[5] P. W. Hammond, "A new approach to enhance power quality for medium voltage drives," *IEEE Trans. Ind. Appl.*, vol. 33, no. 1, pp. 202–208, Jan./Feb. 1997.

[6] Z. Ni, A. H. Abuelnaga, and M. Narimani, "A new fault-tolerant technique based on nonsymmetrical selective harmonic elimination for cascaded H-bridge motor drives," *IEEE Trans. Ind. Electron.*, vol. 68, no. 6, pp. 4610–4622, Jun. 2021, doi: 10.1109/TIE.2020.2989705.

[7] D. Paice, *Power Electronics Converter Harmonics: Multipulse Methods for Clean Power*. Hoboken, NJ, USA: Wiley, 1999.

[8] *IEEE Recommended Practice and Requirements for Harmonic Control in Electric Power Systems*, IEEE Std 519-2014 (Revision of IEEE Std 519-1992), Jun. 2014.

[9] G. S. Kulothungan, A. Edpuganti, A. K. Rathore, J. Rodriguez, and D. Srinivasan, "Hybrid SVM-SOPWM modulation of current-fed three level inverter for high power application," *IEEE Trans. Ind. Appl.*, vol. 55, no. 4, pp. 4344–4358, Jul./Aug. 2019, doi: 10.1109/TIA.2019.2912967.

[10] J. Rodriguez et al., "Design and evaluation criteria for high power drives," in *Proc. IEEE Ind. Appl. Soc. Annu. Meeting*, 2008, pp. 1–9, doi: 10.1109/08IAS.2008.341.

[11] J. Rodriguez, J. Pontt, N. Becker, and A. Weinstein, "Regenerative drives in the megawatt range for high-performance downhill belt conveyors," *IEEE Trans. Ind. Appl.*, vol. 38, no. 1, pp. 203–210, Jan./Feb. 2002.

[12] N. R. Raju, "An SCR-based regenerative converter for VSI drives," in *Proc. IEEE 34th Annu. Conf. Power Electron. Specialist*, 2003, pp. 1770–1774, doi: 10.1109/PESC.2003.1217723.

[13] N. R. Raju, "Regenerative and ride-through capability for AC drives through thyristor-based extensions of the diode front-end," in *Proc. 38th IAS Annu. Meeting Conf. Rec. Ind. Appl. Conf.*, 2003, pp. 1571–1575, doi: 10.1109/IAS.2003.1257765.

[14] M. Malinowski, K. Gopakumar, J. Rodriguez, and M. A. Pérez, "A survey on cascaded multilevel inverters," *IEEE Trans. Ind. Electron.*, vol. 57, no. 7, pp. 2197–2206, Jul. 2010, doi: 10.1109/TIE.2009.2030767.

[15] M. A. Pérez, J. R. Espinoza, J. R. Rodríguez, and P. Lezana, "Regenerative medium-voltage AC drive based on a multicell arrangement with reduced energy storage requirements," *IEEE Trans. Ind. Electron.*, vol. 52, no. 1, pp. 171–180, Feb. 2005.

[16] P. W. Hammond, "Four-quadrant AC-AC drive and method," U.S. Patent No. 6,166,513. Dec. 2000.

[17] A. Yazdani and R. Iravani, *Voltage-Sourced Converters in Power Systems*. Hoboken, NJ, USA: Wiley, 2010.

[18] R. Teodorescu, M. Liserre, and P. Rodriguez, *Grid Converters for Photovoltaic and Wind Power Systems*. Hoboken, NJ, USA: Wiley, 2011.

[19] Z. Ni et al., "A new approach to input filter design for regenerative cascaded H-bridge (CHB) drives," *IEEE Trans. Ind. Electron.*, vol. 69, no. 4, pp. 3266–3277, Apr. 2022, doi: 10.1109/TIE.2021.3071694.

[20] A. Edpuganti and A. K. Rathore, "A survey of low switching frequency modulation techniques for medium-voltage multilevel converters," *IEEE Trans. Ind. Appl.*, vol. 51, no. 5, pp. 4212–4228, Sep./Oct. 2015, doi: 10.1109/TIA.2015.2437351.

[21] J. Napoles, J. I. Leon, R. Portillo, L. G. Franquelo, and M. A. Aguirre, "Selective harmonic mitigation technique for high-power converters," *IEEE Trans. Ind. Electron.*, vol. 57, no. 7, pp. 2315–2323, Jul. 2010, doi: 10.1109/TIE.2009.2026759.

[22] A. K. Rathore, J. Holtz, and T. Boller, "Synchronous optimal pulsewidth modulation for low-switching-frequency control of medium-voltage multilevel inverters," *IEEE Trans. Ind. Electron.*, vol. 57, no. 7, pp. 2374–2381, Jul. 2010, doi: 10.1109/TIE.2010.2047824.

[23] T. Geyer, N. Oikonomou, G. Papafotiou, and F. D. Kieferndorf, "Model predictive pulse pattern control," *IEEE Trans. Ind. Appl.*, vol. 48, no. 2, pp. 663–676, Mar./Apr. 2012, doi: 10.1109/TIA.2011.2181289.

[24] V. E. Wagner, A. A. Andreshak, and J. P. Staniak, "Power quality and factory automation," *IEEE Trans. Ind. Appl.*, vol. 26, no. 4, pp. 620–626, Jul./Aug. 1990, doi: 10.1109/28.55984.

[25] A. von Jouanne, P. N. Enjeti, and B. Banerjee, "Assessment of ride-through alternatives for adjustable-speed drives," *IEEE Trans. Ind. Appl.*, vol. 35, no. 4, pp. 908–916, Jul./Aug. 1999, doi: 10.1109/28.777200.

[26] *IEEE Standard for Performance of Adjustable-Speed AC Drives Rated 375 kW and Larger*, IEEE Std 1566-2015 (Revision of IEEE Std 1566-2005), Feb. 2015, pp. 1–74, doi: 10.1109/IEEESTD.2015.7051199.

[27] J. L. Duran-Gomez, P. N. Enjeti, and B. O. Woo, "Effect of voltage sags on adjustable-speed drives: A critical evaluation and an approach to improve performance," *IEEE Trans. Ind. Appl.*, vol. 35, no. 6, pp. 1440–1449, Nov./Dec. 1999, doi: 10.1109/28.806060.

[28] M. Abolhassani, "Modular multipulse rectifier transformers in symmetrical cascaded H-bridge medium voltage drives," *IEEE Trans. Power Electron.*, vol. 27, no. 2, pp. 698–705, Feb. 2012, doi: 10.1109/TPEL.2011.2161593.

[29] M. Kale and E. Ozdemir, "A novel adaptive hysteresis band current controller for shunt active power filter," in *Proc. IEEE Conf. Control Appl.*, 2003, pp. 1118–1123, doi: 10.1109/CCA.2003.1223167.

[30] "Current-controlled thyristor rectifier," Current-Controlled Thyristor Rectifier—MATLAB & Simulink, MALTAB, 2022, [Online]. Available: https://www.mathworks.com/help/physmod/sps/ug/current-controlled-thyristor-rectifier.html

[31] Z. Ni, M. Narimani, and N. R. Zargari, "Optimal LCL filter design for a regenerative cascaded H-bridge (CHB) motor drive," in *Proc. IEEE Energy Convers. Congr. Expo.*, 2020, pp. 3038–3043, doi: 10.1109/ECCE44975.2020.9235427.

[32] Z. Ni, A. Abuelnaga, M. Narimani, and N. R. Zargari, "DC-link voltage ripple control of regenerative CHB drives for capacitance reduction," *IEEE Trans. Ind. Electron.*, vol. 69, no. 4, pp. 3245–3254, Apr. 2022, doi: 10.1109/TIE.2021.3076727.

[33] Z. Ni, M. Narimani, and N. R. Zargari, "SCR-front-end regenerative CHB drive with improved harmonic profile," in *Proc. IEEE Energy Convers. Congr. Expo.*, 2022.

Zhituo Ni (Member, IEEE) received the Ph.D. degree in electrical engineering from the McMaster University, Hamilton, ON, Canada, in 2021.

He is currently a Sessional Lecturer with the Department of Electrical and Computer Engineering, McMaster University, Hamilton, ON, Canada. He is also a Power Electronics Engineer with the Rockwell Automation, Cambridge, ON, Canada. His research interests include multilevel power converters, grid-interfaced converters, motor drives, and machine learning in power electronics.

Dr. Ni served as a Sessional Chair for IEEE ECCE conference.

Ahmed H. Abuelnaga (Member, IEEE) received the B.Sc. (Hons.) and M.Sc. degrees in electrical engineering from the Ain Shams University, Cairo, Egypt, in 2012 and 2017, respectively, and the Ph.D. degree in electrical engineering from the McMaster University, Hamilton, ON, Canada, in 2021.

From 2012 to 2017, he was a Teaching Staff with the Department of Electrical Power and Machines, Ain Shams University. From 2018 to 2021, he was in collaboration with the Research and Development, Rockwell Automation Inc., Cambridge, ON, Canada. He is currently a Control Firmware Engineer with the Rockwell Automation Inc. His research interests include power electronics interfaces, motor drives, embedded control, reliability, and predictive maintenance.

Sarah Badawi (Student Member, IEEE) received the bachelor's degree in electrical engineering from the Ain Shams University, Cairo, Egypt, in 2016, and the master's degree in power electronics from the McMaster University, Hamilton, ON, Canada, in 2020.

From Sep. 2018 to Aug. 2022, she has been a Research Assistant with the High Power Electronics Lab, McMaster University, and has been working in collaboration with the R&D, Rockwell Automation, Cambridge, ON, Canada to develop new generations of motor drives. Her research interests include EV extreme fast charging systems, grid-connected systems, high-power multilevel inverters, motor drives, and power electronics converters control.

Shaoyi Yuan received the B.Eng. degree in automation from the Northeastern University, Qinhuangdao, China, in 2018, and the M.A.Sc. degree in electrical and computer engineering from the McMaster University, Hamilton, ON, Canada, in 2020.

He is currently working as a Power Electronics Engineer with the Schneider Electric, Shanghai, China, focusing on hardware design, validation, and verification for low-voltage variable speed drives. His research interests include grid-tied power converters, motor control, model-based design of functional circuit test prototype, and optimization for power electronics.

Mehdi Narimani (Senior Member, IEEE) received the Ph.D. degree in electrical engineering from the University of Western Ontario, London, ON, Canada, in 2012.

He is currently an Associate Professor with the Department of Electrical and Computer Engineering, and the University Scholar with the McMaster University, Hamilton, ON, Canada. He also holds the NSERC Canada Research Chair position in high-power converter systems. Prior joining the McMaster University, he was a Power Electronics Engineer with the Rockwell Automation Canada, Cambridge, ON, Canada. He has authored/coauthored more than 150 journals and conference proceeding papers, coauthored a Wiley-IEEE Press book, and holds eight issued/pending U.S./European patents. His research includes power conversion, control of power electronics converters, fast EV Chargers, and wireless EV charging systems.

Dr. Narimani has been an Associate Editor for IEEE TRANSACTIONS ON POWER ELECTRONICS, IEEE TRANSACTIONS ON VEHICULAR TECHNOLOGY, and vice chair and topic char for top tier conferences such as IEEE Energy Conversion Congress and Exposition and IEEE Applied Power Electronics conference and Exhibition.

Ahmed Sayed-Ahmed (Senior Member, IEEE) received the B.Sc. and M.Sc. degrees in electrical engineering from the Cairo University, Giza, Egypt, in 1998 and 2003, respectively, and the Ph.D. degree in electrical engineering from the Marquette University, Milwaukee, WI, USA, in 2009.

He is currently a Principal Engineer (2009–present). He has more than 18 years of industrial/research experience that include control and design of power converters, embedded real-time control systems applied to power electronic applications, power system analysis, and oil and gas industry. Before joining the Rockwell Automation, he worked as a Senior Electrical Engineer with the Rashid Petroleum Company "British Gas joint venture," Maadi, Egypt, from 2000 to 2005. He has taught in several prestigious universities, such as Marquette University and the University of Milwaukee School of Engineering, where he is currently teaching several graduate and undergraduate classes in the areas of control design, power electronics, and electrical machines. His technical and academic record resulted in an honorable list of 23 peer-reviewed journal and conference publications with more than 230 citations, 25 granted patents, and 25 pending patent applications. His research interests include commissioning, startup, and troubleshooting of electrical equipment on onshore and on offshore platforms.

Dr. Sayed-Ahmed is the recipient of the IEEE Power and Energy Society Transaction Prize Paper award for the year of 2012. He is currently serving as a chapter chair for the IEEE POWER ELECTRONICS SOCIETY, Milwaukee section.

Zhongyuan Cheng (Senior Member, IEEE) received the M.A.Sc. degree in electrical and computer engineering from the Ryerson University, Toronto, ON, Canada, in 2005, and the Ph.D. degree in electrical engineering from the Huazhong University of Science and Technology, Wuhan, China, in 1995.

In 2006, he joined the Rockwell Automation Canada, Cambridge, ON, Canada. He is currently working on medium-voltage drive topologies, power electronics design, and motor drive control. His research interests include new converter topologies and the control of high-power medium-voltage drives, the integration and applications of medium-voltage industrial drives: drive-utility interactions, the application of MV drives in generator systems, and drive stability issues in special applications.

Navid R. Zargari (Fellow, IEEE) received the B.Eng. degree in electrical engineering from the Tehran University, Tehran, Iran, in 1987, and the M.A.Sc. and Ph.D. degrees in electrical engineering from the Concordia University, Montreal, QC, Canada, in 1991 and 1995 respectively.

He has been with the Rockwell Automation Canada, since 1994, first as a Senior Designer, then as the Manager of Medium Voltage R&D, and currently as the Senior manager of Power & Control Architecture Group. For the past 25 years, he has been involved with simulation, analysis, and design of power converters for medium-voltage ac drives. He has coauthored more than 100 research papers and two books: "Power Conversion and Control of Wind Energy Systems" and "Modular Multilevel Converters: Analysis, Control and Applications." He holds more than 40 granted/pending patents in areas of power converters and medium-voltage applications. His research interests include power converter topologies and their control aspects, power semiconductors, and renewable energy sources.

Dr. Zargari is a Co-Editor-in-Chief of IEEE TRANSACTIONS ON POWER ELECTRONICS, an Associate Editor of IEEE OPEN JOURNAL OF POWER ELECTRONICS, and a member of PELS AdCom. He is registered as a Professional Engineer in the Province of Ontario and was the recipient of the Premier's Innovation Award for the Innovator of the year in 2009 from the Province of Ontario in 2009.